Theor Chem Acc (2011) 130:429–438
DOI 10.1007/s00214-011-1019-4

REGULAR ARTICLE

Role of hydrogen bonds in acid-catalyzed hydrolyses of esters

Shinichi Yamabe · Takeshi Fukuda · Misao Ishii

Received: 30 March 2011 / Accepted: 8 August 2011 / Published online: 26 August 2011

Abstract Acid-catalyzed ester hydrolyses were studied by means of DFT calculations. A model composed of ester and $H_3O^+(H_2O)_{15}$ was adopted, and substrates esters are ethyl acetate, ethyl para-X-substituted benzoates (X = O_2N, Cl, H, iso-Bu, MeO, and Me_2N), and isobutyl benzoate. For the ethyl acetate, a stepwise path, precursor → TS1 → Int1 → Int2 → TS2 → product, was obtained. Here, TS is the transition state, and Int is the tetrahedral intermediate. The path is somewhat different from the established $A_{AC}2$ mechanism; the carbocation intermediate was calculated to be absent in the present model. The absence holds even for benzoates that may stabilize the cation except the X = Me_2N substituted one. At each local energy minimum, the cation character is retained in H_3O^+. Proton relays along hydrogen bonds were found to prompt interchanges of covalent bonds. The rate-determining step is either TS1 for the electron-withdrawing X or TS2 for the electron-donating one.

Keywords Ester · Acid-catalyzed · Hydrolyses · DFT calculations · Ethyl acetate · Ethyl benzoates · Transition state · Hydrogen bond

Dedicated to Professor Shigeru Nagase on the occasion of his 65th birthday and published as part of the Nagase Festschrift Issue.

Electronic supplementary material The online version of this article (doi:10.1007/s00214-011-1019-4) contains supplementary material, which is available to authorized users.

S. Yamabe (✉) · T. Fukuda · M. Ishii
Department of Chemistry, Nara University of Education, Takabatake-cho, Nara-shi 630-8528, Japan
e-mail: yamabes@nara-edu.ac.jp

1 Introduction

The hydrolysis of esters in the presence of a dilute acid (such as hydrochloric acid or sulfuric acid) is a well-known reaction as (1) shows [1–4].

$$R-CO-OR' + H_2O \longrightarrow^{H^+} R-CO-OH + HO-R' \quad (1)$$

Ethyl acetate, $H_3C–COOC_2H_5$, is a typical ester for the hydrolysis. Ethyl benzoate esters have been also used as reactants to study the kinetics of the hydrolysis [5]. In the water–acetone binary solvent, activation energies of reactions of ethyl benzoate, para-nitrobenzoate, and para-tolyl ethylbenzoate are 20.3, 19.7, and 20.4 kcal/mol, respectively.

The $A_{AC}2$ mechanism of the hydrolysis involving the tetrahedral intermediate [6] seems to be established as depicted in Scheme 1 [7]. By the use of the methanol enriched in the mass 18 isotope of oxygen [8], cleavage of the O=C…OMe bond was proved. The hydrolysis of acyl derivatives like esters and amides with nucleophiles received much attention because of their importance in enzyme-catalyzed reactions [9].

In our previous work, the neutral reaction was examined by the use of a model composed of the ethyl acetate and $(H_2O)n$ (the number of water molecules, n = 1–4, 9, and 16) [10]. The n = 4 based reaction models were found to give likely reaction paths (Scheme 2). A stepwise path via TS1 and TS2 was calculated to be more favorable than a concerted one.

The acid-catalyzed hydrolyses of para-substituted benzoate esters in near-critical water (250–300 °C) were investigated [11]. They showed autocatalytic kinetic behavior and unexpectedly gave the same rate constant regardless of the substituent. For the isobutyl benzoate

Scheme 1 The $A_{AC}2$ mechanism traditionally considered for the acid-catalyzed ester hydrolysis. Here, A denotes acid, and the subscript AC indicates acyl-oxygen fission. The digit 2 indicates the bimolecular nature of the rate-determining step. i_a, i_b, i_c, and i_d stand for intermediates

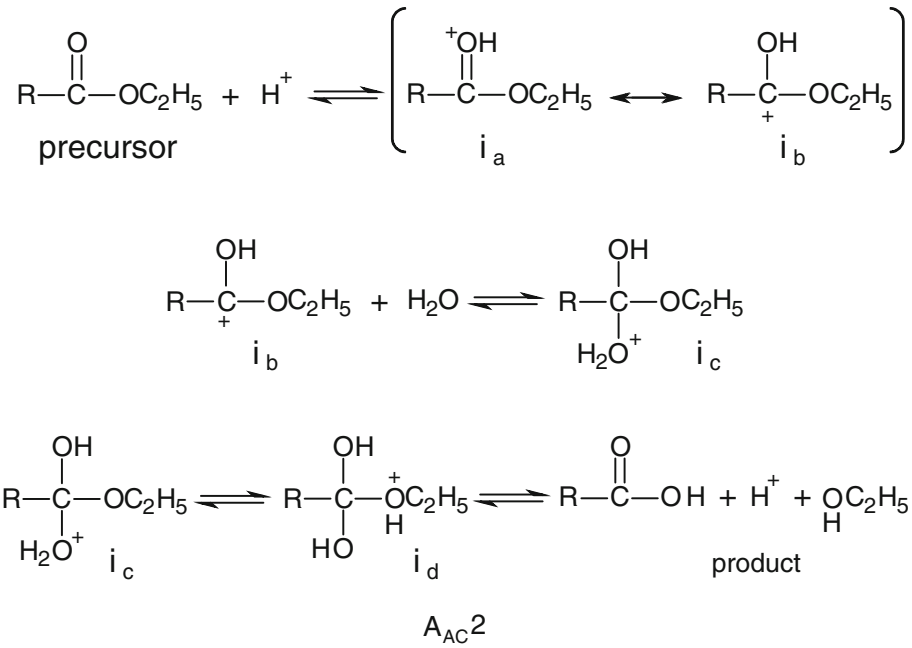

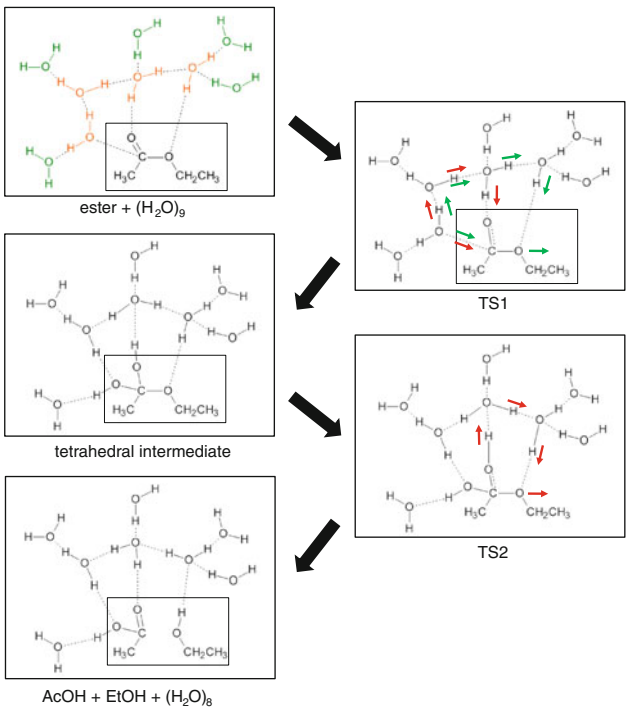

Scheme 2 A reaction scheme of the neutral hydrolysis of ethyl acetate ester reported in our previous work [10]. In ester $+(H_2O)_9$, *four orange color* H_2O molecules stand for reactant ones, and *five green ones* do for catalytic ones. At TS1 and TS2, *red color arrows* show movements for the stepwise process. At TS1, *green color arrows* for the concerted process

substrate, Ph–CO–O(iBu), the activation energy was estimated to be 24.14 ± 3.11 kcal/mol. This value is larger than 19.63 kcal/mol for the reaction of the ethyl benzoate in the ethanol–water solvent [5]. Hydrolyses of para-substituted isobutyl benzoates were reported to be of the acid-catalyzed mechanism [11].

In spite of the well-known reaction, precise pictures of the $A_{AC}2$ mechanism are still unresolved. In particular, movement of the proton along hydrogen bonds in the water cluster needs to be elucidated. Presence or absence of the carbocation intermediate might depend on the electron-donating strength of the substituent R. In this work, the acid-catalyzed ester hydrolyses were studied by means of DFT calculations in order to consider the above questions. Various ester substrates were adopted to examine the presence or absence systematically.

2 Method of calculations

The reacting systems were investigated by density functional theory calculations. The B3LYP method [12, 13] was used. B3LYP seems to be a suitable method, which includes the electron correlation effect to some extent. The basis sets employed were 6-31G(d) and 6-311G(d,p), because the present systems are large (for the largest stoichiometry $C_{13}H_{51}O_{18}(+)$, 895 basis functions of 6-311G(d,p) used in the geometry optimizations) and calculations by the higher-level basis set than 6-311G(d,p) are too difficult. Transition states (TSs) were sought first by partial optimizations at bond interchange regions. Second, by the use of Hessian matrices, TS geometries were optimized. They were characterized by vibrational analyses, which checked whether the obtained geometries have single imaginary frequencies ($\upsilon^{\ddagger}$s). From TSs, reaction paths were traced by the intrinsic reaction coordinate (IRC)

method [14, 15] to obtain the energy-minimum geometries. Relative energies ΔE were obtained by single-point calculations of RB3LYP/6-311+G(d,p) [self-consistent reaction field (SCRF) = PCM, [16–18] solvent = water] on the RB3LYP/6-31G(d) geometries and their ZPVE(zero-point vibration energy) ones. For two TSs, TS1(Me) and TS2(Me), of Fig. 2, RB3LYP/6-31G(d) SCRF = PCM, RB3LYP/6-311+G(d,p), and M062x/6-311G(d,p) [19] optimizations and the subsequent IRC calculations were also carried out. From the two TSs, classical trajectory calculations using the atom-centered density matrix propagation molecular dynamics (ADMP) model [20–22] were conducted.

All the calculations were carried out using the GAUSSIAN 09 [23] program package. The computations were performed at the Research Center for Computational Science, Okazaki, Japan.

3 Results and discussions

3.1 Hydrolysis of ethyl acetate (R = H_3C)

Scheme 3 shows the way of constructing models of (a) neutral and (b) acid-catalyzed reactions. They are composed of ester$(H_2O)_{16}$ and ester$(H_3O^+)(H_2O)_{15}$, respectively, and are isoelectronic. Lone-pair orbitals of carbonyl and acyl oxygen are connected to the water cluster by hydrogen bonds. As a reference to the acid-catalyzed reactions studied in this work, the neutral one ("−N") was re-examined first on the basis of Scheme 3a. In the previous study [10], only TS1 and TS2 were reported and IRC calculations were not performed. Their results are shown in Figure S1 (Supporting Information). In the Figure, the stepwise path is exhibited. Likewise, on the basis of Scheme 3b, acid promoted paths were sought. Figure 1 shows the calculated concerted path. The reactant like complex is "precursor-a(Me)." From it, TS(Me) was obtained. After TS(Me), ethanol and acetic acid molecules are evolved at "product-a(Me)." The concerted path in Fig. 1 is different from the $A_{AC}2$ mechanism in Scheme 1 and would be less favorable than the stepwise one. However, as far as the two paths coexist, their superiority or inferiority needs to be examined on an equal footing.

Figure 2 exhibits geometric changes along the stepwise path. From precursor-b(Me), TS1(Me) was obtained. After TS1(Me), the tetrahedral intermediate Me–C$(OH)_2$–OEt, Int1(Me), was brought about. Noteworthy is that the carbocation i_b in Scheme 1 was not found. The cation character is retained in H_3O^+. The hydronium ion may be shifted along O–H…O hydrogen bonds, and the conversion of Int1(Me) to Int2(Me) around Me–C$(OH)_2$–OEt is a facile process. From Int2(Me), product-b(Me) was afforded

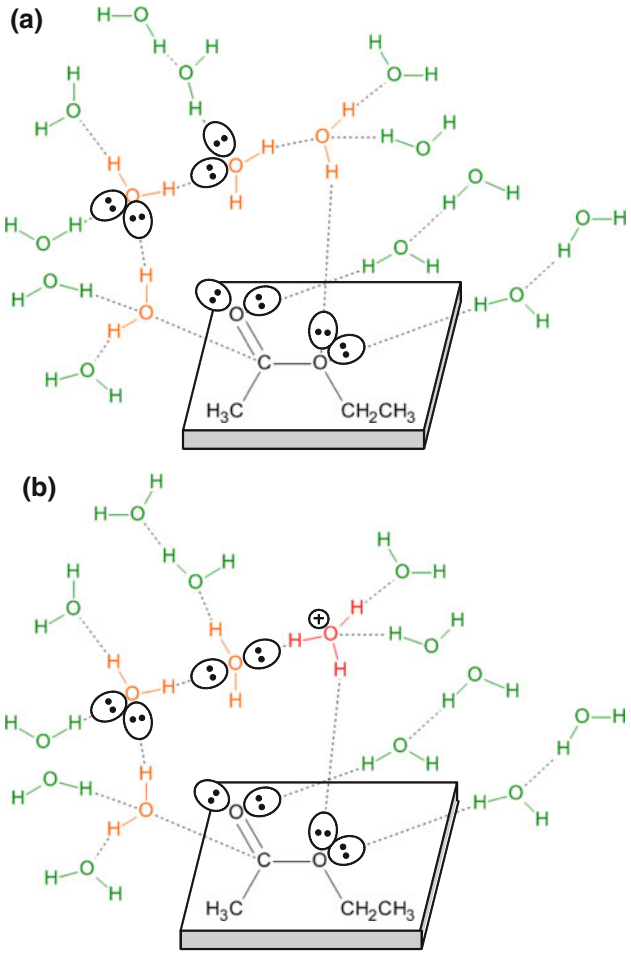

Scheme 3 Model construction to seek (**a**) neutral and **b** acid-catalyzed reaction paths

via TS2(Me). Main distances in TS1(Me) and TS2(Me) are shown in Table 1. The stepwise path shown in Fig. 2 is somewhat different from the $A_{AC}2$ mechanism. The difference was examined by the other three DFT methods, RB3LYP/6-31G(d) SCRF = PCM, RB3LYP/6-311+G(d,p), and M062x/6-311G(d,p). Their results of TS1(Me) and TS2(Me) are displayed in Table 1. IRC calculations by the three methods gave the same stepwise paths as those by RB3LYP/6-31G(d) and RB3LYP/6-311G(d,p). In the present large system, Me–CO–OEt + $H_3O^+(H_2O)_{15}$, there would be many local minima. Dynamical calculations of RB3LYP/6-31G(d) ADMP on TS1(Me) and TS2(Me) were carried out. Geometries at 2,000 steps in 0.1-femtosecond time step from TS1(Me) to TS2(Me) are shown as ADMP-1 and ADMP-2, respectively, in Figure S7 (Supporting Information). The geometry of ADMP-1 is almost the same as that of precursor-b(Me) in Fig. 2. Also, the geometry of ADMP-2 is close to that of Int2(Me). Thus, the present stepwise path seems to be meaningful.

Intervention of the carbocation i_a or i_b (Scheme 1) was examined by a model composed of the protonated ester and

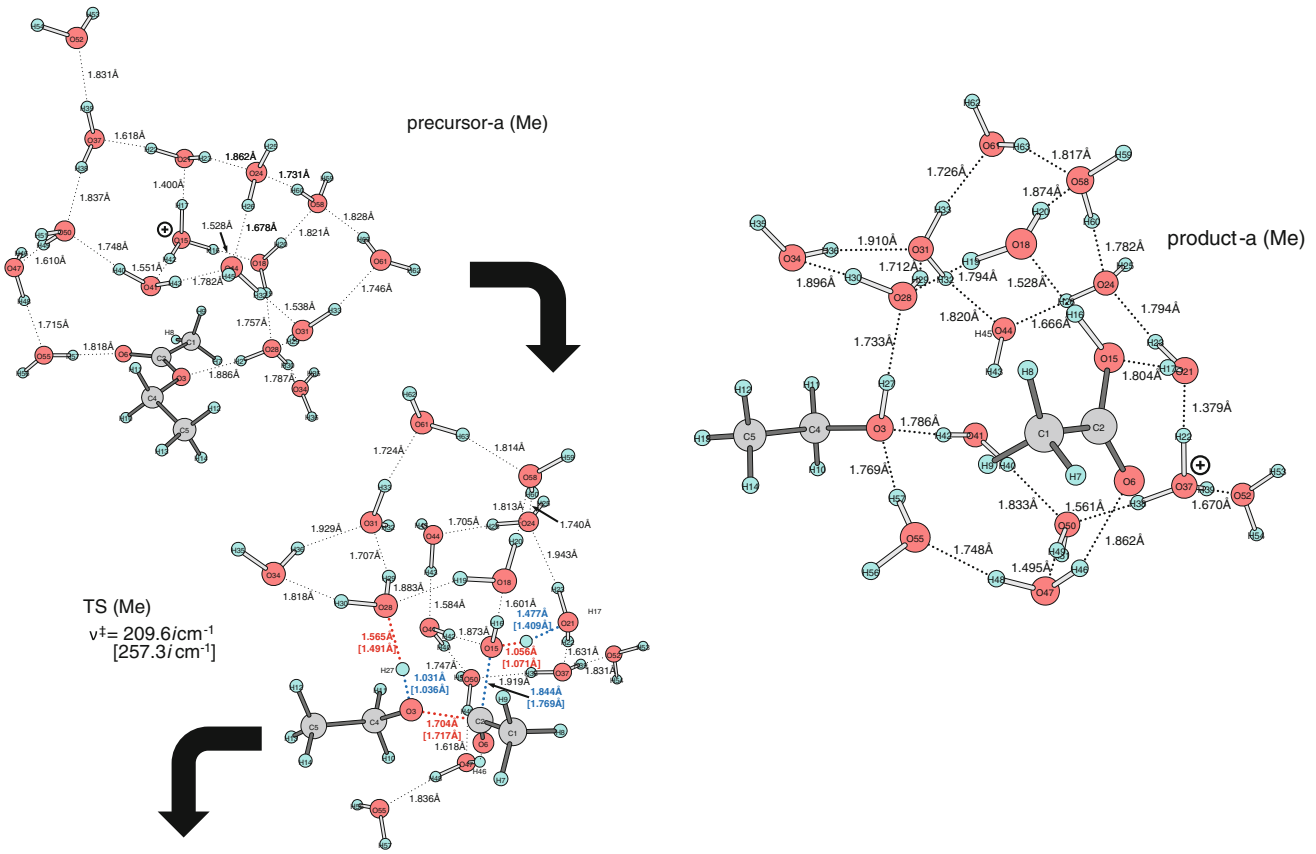

Fig. 1 Geometric changes for the concerted path of $H_3C–COOC_2H_5 + H_3O^+(H_2O)_{15} \rightarrow H_3C–COOH + HO–C_2H_5 + H_3O^+(H_2O)_{14}$. The symbol (Me) stands for R = Me in the R–COOEt substrate. At TS(Me), *red* and *blue dotted lines* show covalent bonds cleaved and formed, respectively. Bond distances without and with square brackets are of B3LYP/6-31G(d) and B3LYP/6-311G(d,p), respectively

$(H_2O)_7$. Its assumed geometry is shown in the upper of Figure S8 (Supporting Information). An optimization of the initial geometry leads to the form of ester and $H_3O^+(H_2O)_6$ in the lower. The calculated result means that the water cluster is a stronger proton acceptor than the ester.

Figure 3 shows energy changes along the acid-catalyzed concerted and stepwise paths. Those of the neutral stepwise one are also exhibited. TS(Me) of the concerted path has a large activation energy (=+40.18 kcal/mol). The path was confirmed to be unlikely. Those of the stepwise paths indicate the catalytic effect on activation energies ($\Delta E^{\ddagger}$s). For the acid-catalyzed reaction, TS2(Me) is the rate-determining step with $\Delta E^{\ddagger} = +19.18$ kcal/mol. This calculated value is somewhat larger than the experimental one, 16.20 kcal/mol [5]. The deviation will be discussed in the next sub-section by the use of the isobutyl benzoate substrate. The small energy difference between precursor-b(Me) and product-b(Me), 0.734 kcal/mol, corresponds to the reversibility of the hydrolysis.

As far as the present model of ester $H_3O^+(H_2O)_{15}$ is concerned, the geometric changes in Fig. 2 have a feature different from the $A_{AC}2$ mechanism. It is necessary to examine whether the difference holds for the other ester substrates.

3.2 Hydrolysis of ethyl benzoates (R = aryl)

Figure 4 exhibits geometric changes of the stepwise reaction of ethyl benzoate (R = Ph). They were found to be similar to those in Fig. 2 (R = Me). The process, precursor(Ph) → TS1(Ph) → Int1(Ph) → Int2(Ph) → TS2(Ph) → product(Ph), is composed of bond interchanges and concomitant proton relays along hydrogen bonds. The carbocation intermediate (i_b in Scheme 1) was not formed in spite of its stability through the resonance inside the phenyl ring. The cation H_3O^+ is retained in precursor(Ph), Int1(Ph), Int2(Ph), and product(Ph). Energy changes (ΔEs) are also shown in Fig. 4 and indicate that TS2 with $\Delta E^{\ddagger} = 25.10$ kcal/mol is the rate-determining step. It is only slightly larger than $\Delta E^{\ddagger}$ of TS1 (=+24.90 kcal/mol). The former value is larger than the experimental one, 19.63 kcal/mol [5]. In order to evaluate the reliability of the calculated activation energy, a reaction of the similar substrate, the isobutyl benzoate [Ph–CO–OCH(Me)(Et)],

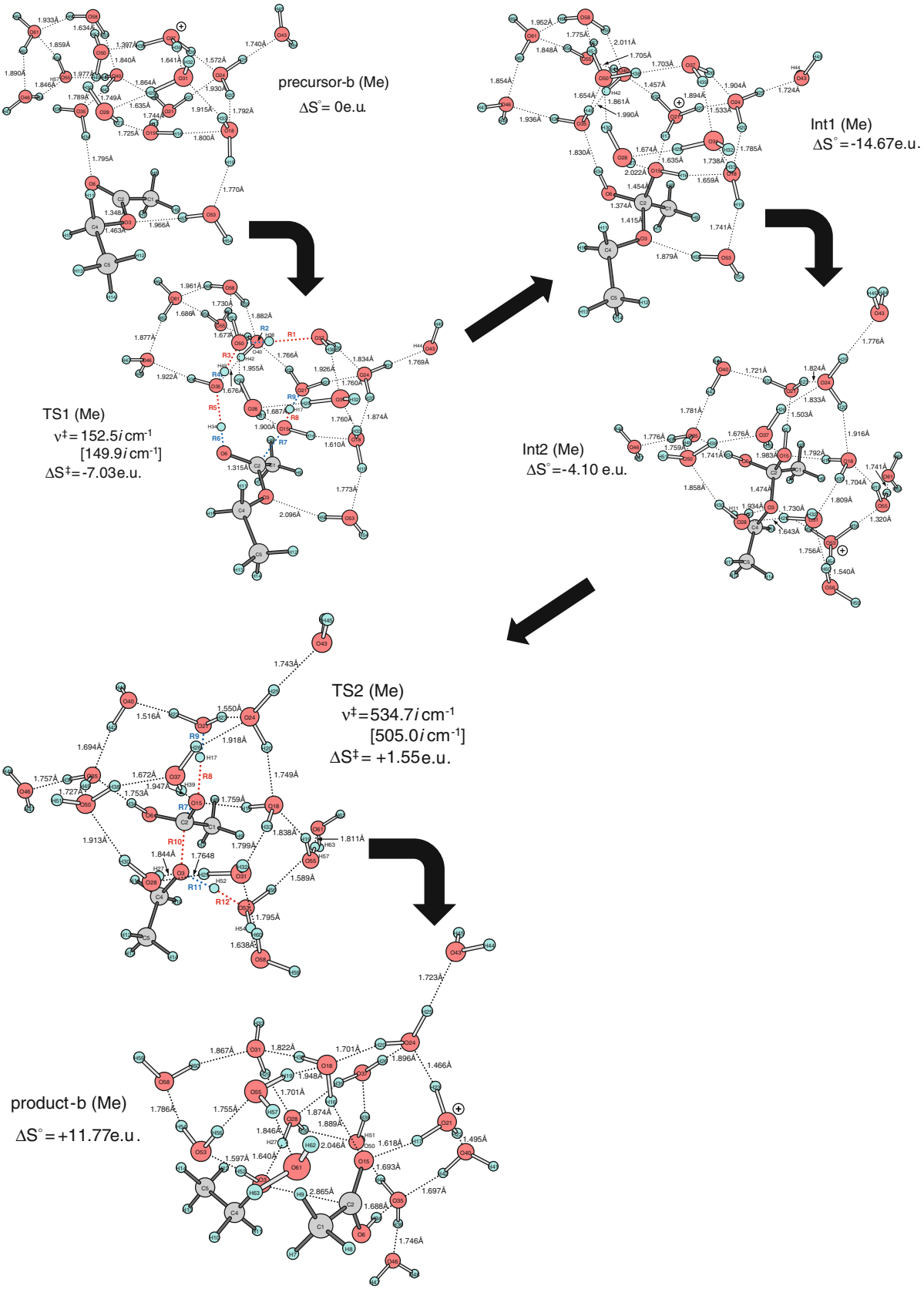

Fig. 2 Geometric changes for the stepwise path. Main distances, R1–R12, depicted in TS1(Me) and TS2(Me) are given in Table 1. ΔS° and $\Delta S^{\ddagger}$ are entropy changes in cal/(mol K) calculated by RB3LYP/6-311+G(d,p)

Table 1 Main distances (R1–R12 in Å) and sole imaginary frequencies ($\upsilon^{\ddagger}$s in cm^{-1}) in TS1(Me) and TS2(Me) of Fig. 2 calculated by 5 methods

Figure 2	Distances and $\upsilon^{\ddagger}$s	B3LYP/ 6-31G(d)	B3LYP/ 6-311G(d,p)	B3LYP/6-31G(d) SCRF = PCM	B3LYP/ 6-311+G(d,p)	M062x/ 6-311G(d,p)
TS1 (Me)	R1	1.698	1.733	1.734	1.775	1.720
	R2	1.002	0.989	0.999	0.986	0.983
	R3	1.603	1.654	1.695	1.690	1.546
	R4	1.023	1.004	1.005	1.000	1.019
	R5	1.582	1.629	1.600	1.677	1.457
	R6	1.022	1.004	1.019	0.998	1.038
	R7	1.833	1.745	1.784	1.699	1.879
	R8	1.050	1.045	1.045	1.056	1.013
	R9	1.508	1.485	1.531	1.456	1.568
	$\upsilon^{\ddagger}$	152.5 *i*	149.9 *i*	181.6 *i*	132.2 *i*	202.3 *i*
TS2 (Me)	R7	1.311	1.314	1.309	1.327	1.296
	R8	1.491	1.417	1.527	1.062	1.416
	R9	1.049	1.066	1.039	1.422	1.052
	R10	1.791	1.743	1.771	1.747	1.788
	R11	1.225	1.234	1.291	1.073	1.084
	R12	1.207	1.182	1.156	1.400	1.343
	$\upsilon^{\ddagger}$	534.7 *i*	505.9 *i*	582.0 *i*	169.6 *i*	188.6 *i*

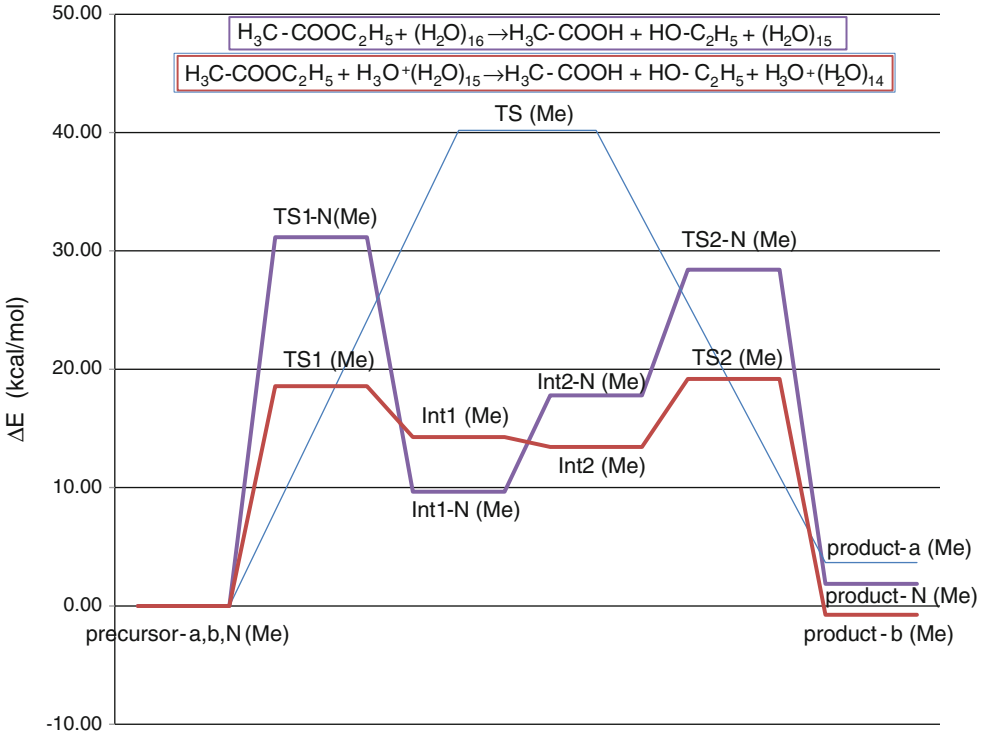

Fig. 3 Energy changes of concerted (Fig. 1) and stepwise (Fig. 2) acid-catalyzed paths calculated by B3LYP/6-311+G(d,p) SCRF = PCM// B3LYP/6-31G(d). Those of the neutral one (Figure S1) are also shown by the sign "−N"[e.g., TS1-N(Me)]. ΔE is the energy difference of the sum of the B3LYP/6-31G(d) zero-point vibration energy and the single-point B3LYP/6-311+G(d,p) SCRF = PCM electronic energy

was investigated. Its activation energy, 24.13 ± 3.11 kcal/mol, was obtained by the acid-catalyzed hydrolysis in near-critical water [11]. Figure S2 in Supporting Information shows the calculated results. TS2 < Ph–CO–O(iBu)> is the rate-determining step with $\Delta E^{\ddagger} = +26.91$ kcal/mol. This value is in the range of the experimental one, and the calculated energies would be meaningful.

Substituent effect of the para position of the benzoate ester on the activation energy was investigated. Substituents adopted are methoxy(MeO), isobutyl(iBu), chloro(Cl), and nitro(O_2N) groups. TS1 and TS2 of these benzoates are shown in Figures S3(MeO), S4(iBu), S5(Cl), and S6(O_2N) in Supporting Information. The four substituents give TS geometries similar to that of the parent benzoate ester

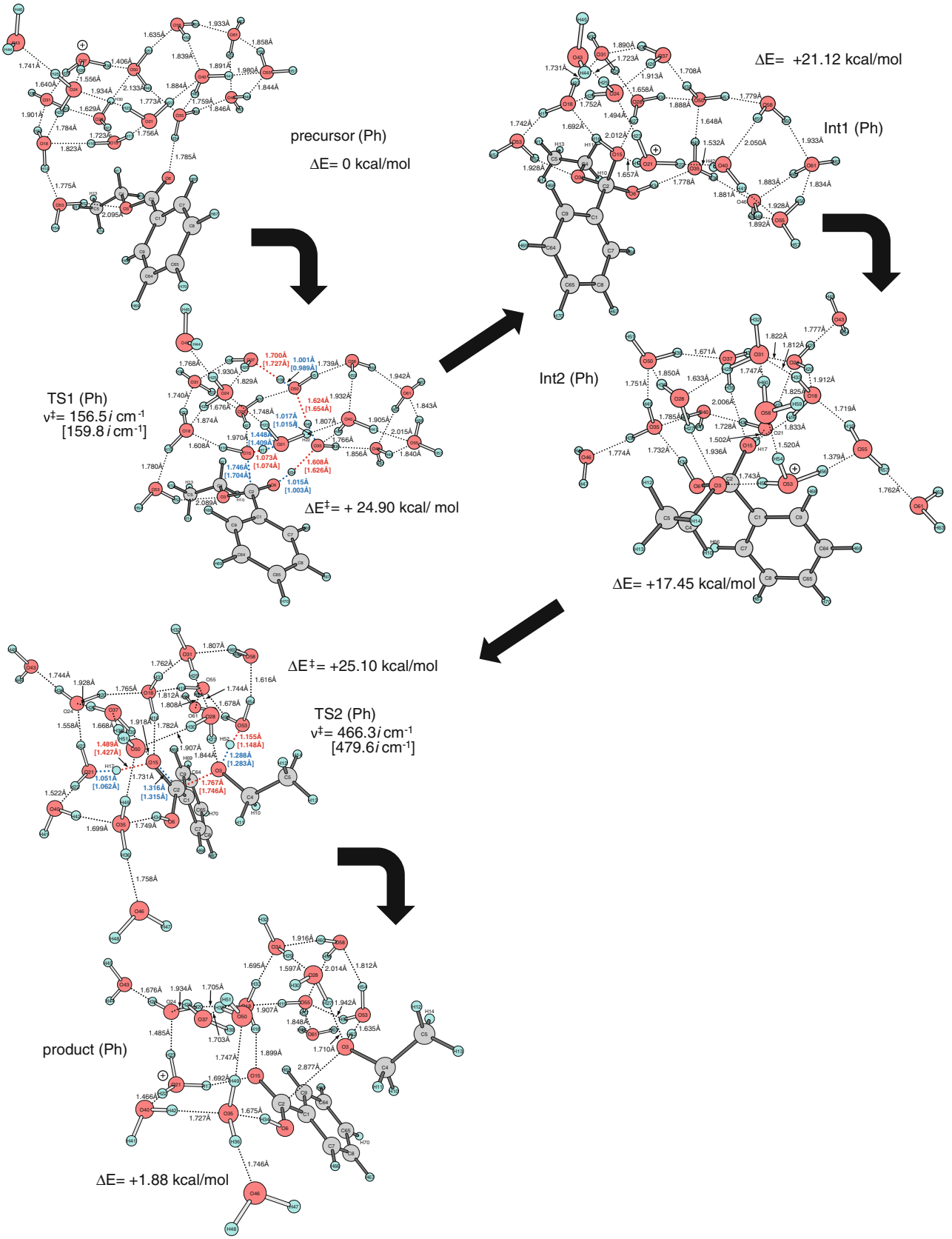

Fig. 4 The stepwise path of the acid-catalyzed hydrolysis of ethyl benzoate. ΔEs are energy changes

(Fig. 4). Through IRC calculations, the processes, precursor → TS1 → Int1 → Int2 → TS2 → product, were again obtained. The carbocation i_b was not found in hydrolyses of those para-substituted benzoate esters.

For ester substrates with electron-donating para substituents, MeO and iBu, $\Delta E^{\ddagger}$(TS2)s are slightly larger than $\Delta E^{\ddagger}$(TS1)s, e.g., $\Delta E^{\ddagger}$(TS1) = +25.92 kcal/mol and $\Delta E^{\ddagger}$(TS2) = +26.19 kcal/mol for the MeO substituent in Figure S3. In contrast, for those with electron-withdrawing groups, O_2N and Cl, TS1s were found to be respective rate-determinig steps. Although the cation i_b is absent, its character is involved in TS1, and the electron-donating substituents enhance the character and lower $\Delta E^{\ddagger}$(TS1) values.

It is noteworthy that the activation energies at the rate-determining steps are similar, e.g., $\Delta E^{\ddagger}$(TS2, Ph) = +25.10 kcal/mol (Fig. 4), $\Delta E^{\ddagger}$(TS2, MeO–C_6H_4) = +26.19 kcal/mol (Fig. S3), and $\Delta E^{\ddagger}$(TS1, O2 N–C_6H_4) = +24.44 kcal/mol (Fig. S6). The similarity corresponds to the "surprising same rate constant regardless of substituent" [11] and comes from compensation effect of proton and HO^- affinities (PA and HOA) shown in Fig. 5. In a simple scheme, the tetrahedral intermediate is formed via the addition of both H^+ to the carbonyl oxygen and HO^- to the carbonyl carbon at TS1. Each substituent has superiority or inferiority for PA and HOA, which nearly levels off $\Delta E^{\ddagger}$ values. TS2 is regarded simply as removal of H^+ and EtO^- from the tetrahedral intermediate. Then, in terms of the reverse use of PA and HOA, the leveling off may hold for TS2.

In order to examine possibility of the carbocation i_b, the strongest (in the Hammett constant) electron-donating para substituent, Me_2N, was adopted. The calculated TS geometries are exhibited in Fig. 6. In addition to TS1 and TS2, TS0 was obtained. TS0 is for the proton (H34) transfer to the carbonyl oxygen (O6), which leads to the carbocation, i_b. Thus, as an extreme case, the cation was found to stay prior to formation of the tetrahedral intermediate. For the X = Me_2N para substituent, therefore, the reaction consists of precursor → TS0 → i_b(carbocation) → TS1 → Int1 → Int2 → TS2 → product.

4 Concluding remarks

In this work, the acid-catalyzed ester hydrolyses were studied by means of B3LYP calculations. A model composed of ester and $H_3O^+(H_2O)_{15}$ was adopted to trace the reaction path. Substrates esters are ethyl acetate, ethyl para-X-substituted benzoates (X = O_2N, Cl, H, iso-Bu, MeO, and Me_2N), and isobutyl benzoate. For the ethyl acetate, concerted and stepwise paths were obtained. The stepwise one was confirmed to be much more likely. It was found to be somewhat different from the traditional $A_{AC}2$ mechanism. Typically, the carbocation i_b is absent, and the cation

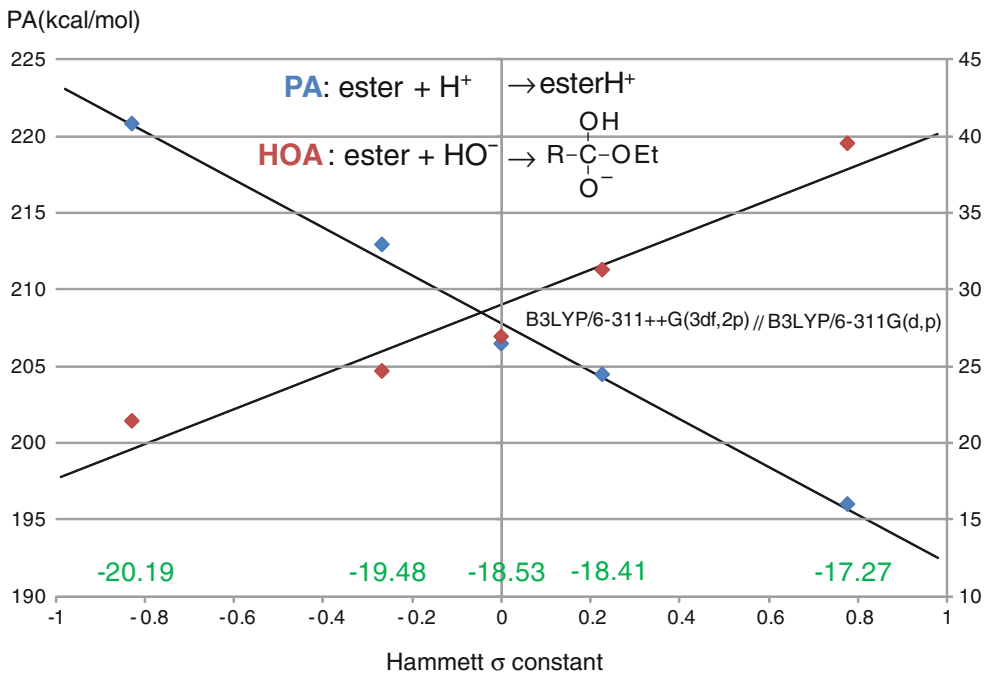

Fig. 5 Correlations of proton (PA) and HO^- (HOA) affinities in kcal/mol with Hammett σ(para) constants. *Green color* negative values denote reaction energies of R–C(=O)–OEt + H_2O ⟶ R–C(OH)(OH)–OEt in kcal/mol

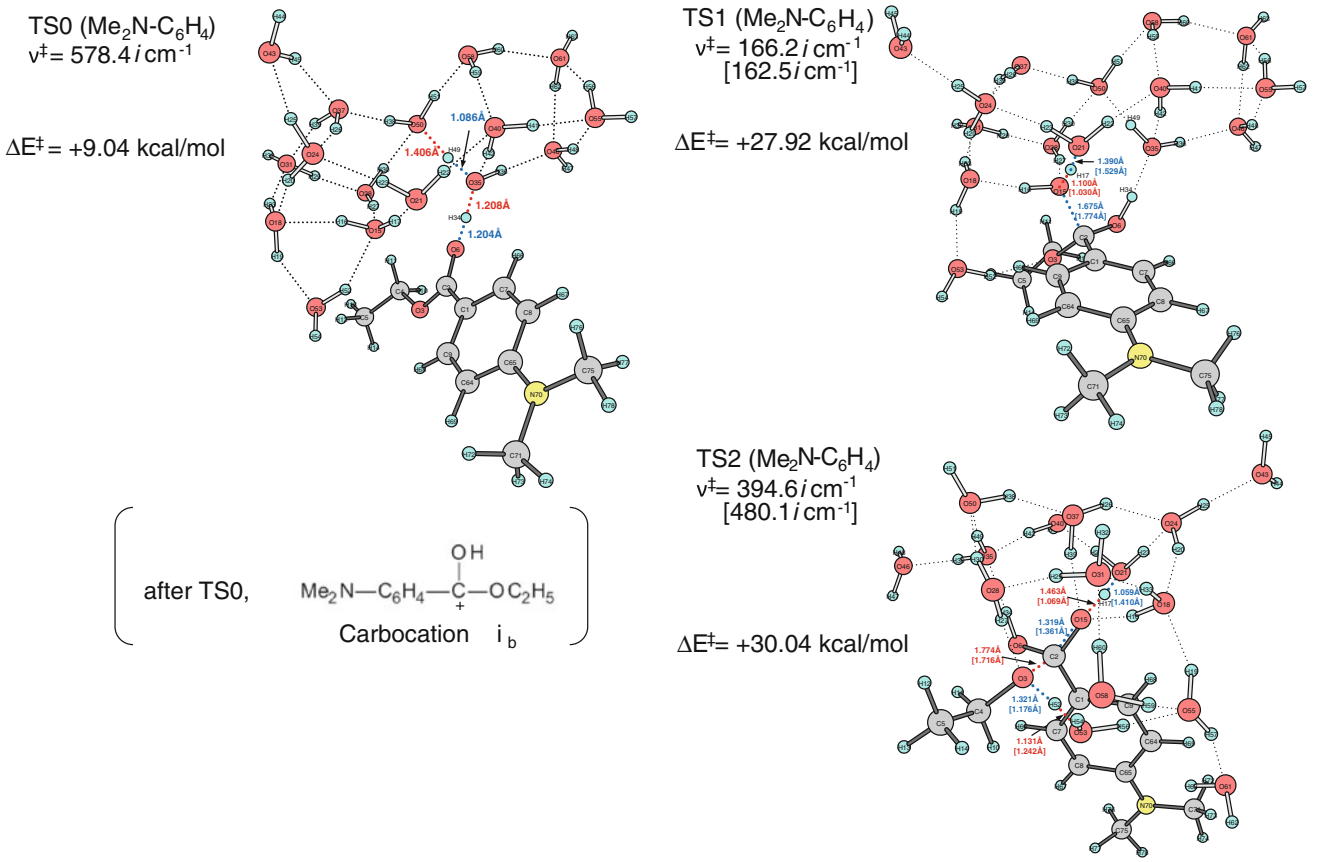

Fig. 6 Three TS geometries of the acid-catalyzed hydrolysis of ethyl para-dimethylaminobenzoate

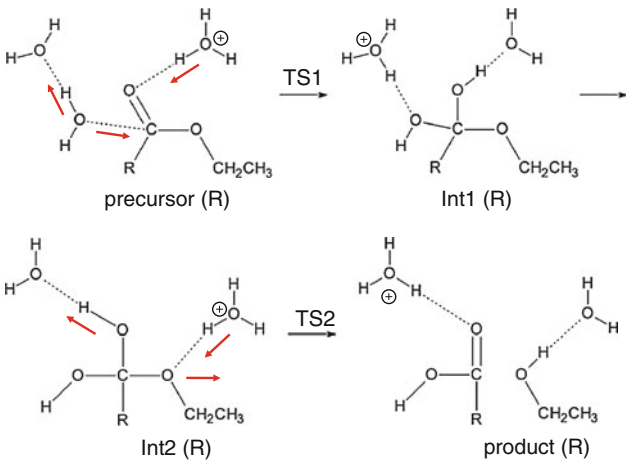

Scheme 4 The suggested stepwise path of the acid-catalyzed ester hydrolysis where the proton attach to the carbon skeleton is precluded except for R = Me_2N–C_6H_4

is retained in H_3O^+ of local energy minima (precursor, tetrahedral intermediate, and product) in the present model of ester $H_3O^+(H_2O)_{15}$. The retention was also obtained for the aryl substrate, although intervention of the carbocation was expected owing to stabilization of canonical resonance structures. Exceptionally, ethyl para-dimethylaminobenzoate gives the cation as an extreme case. Scheme 4 illustrates a minimal model composed of the ester and $H_3O^+(H_2O)_2$, which have been derived from the present calculations. Proton transfers along hydrogen bonds give ready interchanges of covalent bonds for the hydrolysis. It should be noted that the present results were obtained by the cluster model calculations and are not necessarily pertinent to the reactivity in the water solution.

References

1. Solomons TWG (1996) Organic chemistry, 6th edn. Wiley, New York, p 812
2. Datta SC, Day JNE, Ingold CK (1939) J Chem Soc 838
3. Day JNE, Ingold CK (1941) Trans Faraday Soc 37:686
4. Laidler KJ, Landskroener PA (1956) Trans Faraday Soc 52:200
5. Timm EW, Hinshelwood CN (1938) J Chem Soc 862
6. Bender ML (1951) J Am Chem Soc 73:1626
7. Carey FA, Sundberg RJ (1984) Advanced organic chemistry, Part A: structure and mechanisms, chapter 8.4, 2nd edn. Plenum Press, New York and London
8. Roberts I, Urey HC (1938) J Am Chem Soc 60:2391

9. Brown RS, Bennett AJ, Slebocka-Tilk H (1992) Acc Chem Res 25:481
10. Yamabe S, Tsuchida N, Hayashida Y (2005) J Phys Chem A 109:7216
11. Lesutis HP, Glaeser R, Liotta CL, Eckert CA (1999) Chem Commun 2063
12. Becke AD (1993) J Chem Phys 98:5648
13. Lee C, Yang W, Parr RG (1988) Phys Rev B 37:785
14. Fukui K (1970) J Phys Chem 74:4161
15. Gonzalez C, Schlegel HB (1989) J Chem Phys 90:2154
16. Cances E, Mennucci B, Tomasi J (1997) J Chem Phys 107:3032
17. Cossi M, Barone V, Mennucci B, Tomasi J (1998) Chem Phys Lett 286:253
18. Mennucci B, Tomasi J (1997) J Chem Phys 106:5151
19. Zhao Y, Truhlar DG (2008) Theor Chem Acc 120:215
20. Iyengar SS, Schlegel HB, Millam JM, Voth GA, Scuseria GE, Frisch MJ (2001) J Chem Phys 115:10291
21. Schlegel HB, Millam JM, Iyengar SS, Voth GA, Scuseria GE, Daniels AD, Frisch MJ (2001) J Chem Phys 114:9758
22. Schlegel HB, Iyengar SS, Li X, Millam JM, Voth GA, Scuseria GE, Frisch MJ (2002) J Chem Phys 117:8694
23. Frisch MJ, Trucks GW, Schlegel HB, Scuseria GE, Robb MA, Cheeseman JR, Scalmani G, Barone V, Mennucci B, Petersson GA, Nakatsuji H, Caricato M, Li X, Hratchian HP, Izmaylov AF, Bloino J, Zheng G, Sonnenberg JL, Hada M, Ehara M, Toyota K, Fukuda R, Hasegawa J, Ishida M, Nakajima T, Honda Y, Kitao O, Nakai H, Vreven T, Montgomery JA Jr, Peralta JE, Ogliaro F, Bearpark M, Heyd JJ, Brothers E, Kudin KN, Staroverov VN, Kobayashi R, Normand J, Raghavachari K, Rendell A, Burant JC, Iyengar SS, Tomasi J, Cossi M, Rega N, Millam NJ, Klene M, Knox JE, Cross JB, Bakken V, Adamo C, Jaramillo J, Gomperts R, Stratmann RE, Yazyev O, Austin AJ, Cammi R, Pomelli C, Ochterski JW, Martin RL, Morokuma K, Zakrzewski VG, Voth GA, Salvador P, Dannenberg JJ, Dapprich S, Daniels AD, Farkas O, Foresman JB, Ortiz JV, Cioslowski J, Fox DJ (2009) Gaussian 09, revision A. 1. Gaussian, Wallingford, CT